



# In silico studies, synthesis and anticancer activity of novel diphenyl ether-based pyridine derivatives

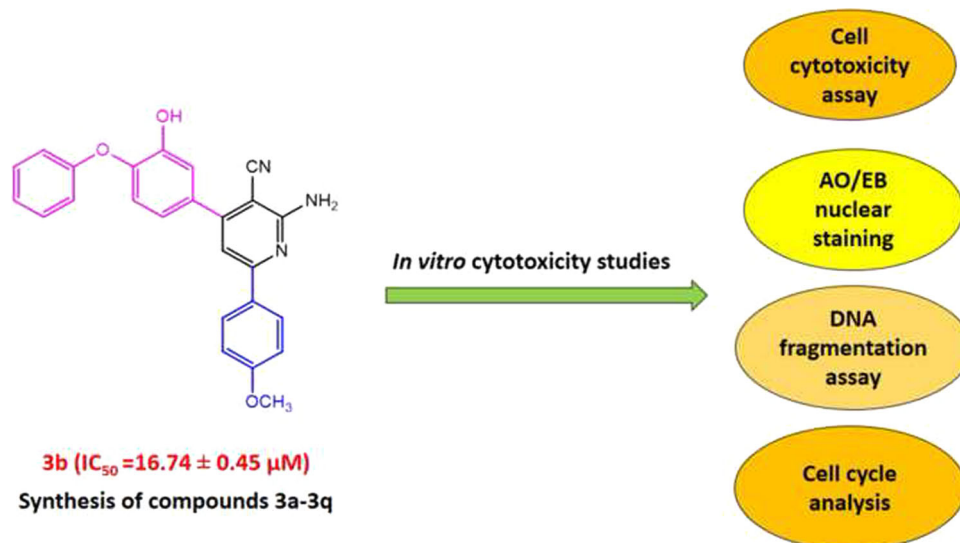
Ruchi Verma<sup>1</sup> · Indira Bairy<sup>2</sup> · Mradul Tiwari<sup>3</sup> · G. Varadaraj Bhat<sup>1</sup> · G. Gautham Shenoy<sup>1</sup>

Received: 26 July 2018 / Accepted: 26 October 2018  
© Springer Nature Switzerland AG 2018

## Abstract

A series of novel 2-amino-4-(3-hydroxy-4-phenoxyphenyl)-6-(4-substituted phenyl) nicotinonitriles were synthesized and evaluated against HepG2, A-549 and Vero cell lines. Compounds **3b** ( $IC_{50}$   $16.74 \pm 0.45 \mu M$ ) and **3p** ( $IC_{50}$   $10.57 \pm 0.54 \mu M$ ) were found to be the most active compounds against A-549 cell line among the evaluated compounds. Further **3b**- and **3p**-induced apoptosis was characterized by AO/EB (acridine orange/ethidium bromide) nuclear staining method and also by DNA fragmentation study. A decrease in cell viability and initiation of apoptosis was clearly evident through the morphological changes in the A-549 cells treated with **3b** and **3p** when stained with this method. Fragmentation of DNA into nucleosomes was observed which further confirmed the cell apoptosis in cells treated with compound **3b**. Flow cytometry studies confirmed the cell cycle arrest at G2/M phase in A549 cells treated with compound **3b**. Further in silico studies performed supported the in vitro anticancer activity of these compounds as depicted by dock score and binding energy values.

## Graphical Abstract



**Keywords** Triclosan · Diphenyl ether derivatives · Human enoyl-acyl carrier protein reductase (hER)

**Electronic supplementary material** The online version of this article (<https://doi.org/10.1007/s11030-018-9889-1>) contains supplementary material, which is available to authorized users.

✉ G. Gautham Shenoy  
gautham.gs@manipal.edu

<sup>1</sup> Department of Pharmaceutical Chemistry, Manipal College of Pharmaceutical Sciences, Manipal Academy of Higher Education, Manipal 576 104, India

## Introduction

Cancer continues to be one of the leading causes of death worldwide in spite of significant knowledge in the understanding of the pathophysiology, treatment, diagnosis and discovery of drugs acting through novel mechanism [1, 2]. Cancer was responsible for 8.8 million deaths worldwide in 2015. It is estimated that the number of new cases will rise by about 70% over the next two decades [3]. As far as the Indian scenario is concerned, the estimated cancer cases for the year 2020 in males are 534,353 and in females, the estimation is approximately 614,404. The total number of cases is expected to reach 1,148,757 in the year 2020 [4].

Novel anticancer agents are associated with severe adverse effects and tumors recurrence. These drawbacks reduce their clinical efficacy. Thus, there is a need to develop new anticancer agents with minimal adverse effects and drug resistance related to chemotherapy [5, 6]. In the past few years, triclosan (TCL) derivatives have gathered a lot of attention as potent anticancer agents and hence we decided to evaluate novel TCL derivatives as anticancer agents [7]. TCL, which is a diphenyl ether derivative, has been reported to target bacterial enoyl-acyl protein reductase and inhibit fatty acid synthase (FASN) through the enoyl-acyl reductase domain [8]. It is evident through literature that TCL is cytotoxic to tumor cells [9]. Human fatty acid synthase is a large multi-domain protein involved in the synthesis of long-chain fatty acids that are usually expressed at very low levels but gets highly upregulated in cancer [10]. Human enoyl-acyl carrier protein reductase (hER) is one among the FAS catalytic domains, and drugs similar to triclosan inhibit hER producing cell toxicity and minimizing drug resistance in cancer cells [8]. TCL as an anticancer agent has been reported to inhibit FASN in various cancer cell lines that include breast cancer cell lines MCF-7, SKBr-3, retinoblastoma Y79 RB cell line, epithelial carcinoma KB cell line and choriocarcinoma JEG-3 cell line [11, 12]. 2-Amino-3-cyanopyridine derivatives have been reported to possess various biological activities such as antimicrobial, anti-parkinsonism, antioxidant, anti-inflammatory, etc. [13]. 2-Amino-3-cyanopyridine derivatives have also exhibited profound anticancer activity against several cell lines. Mohamed et al. synthesized novel 3 cyano-aminopyridine derivatives by reacting 3-indole carboxaldehyde and 3-aminoacetophenone and tested them for anticancer activity in MCF-7 (breast cancer cell line). Some of the compounds exhibited potent anticancer

activity (Fig. 1a) [14]. Few 4-[2-amino-3-cyano-5-oxo-4-substituted aryl-4H-indeno [1, 2-b] pyridin-1-(5H)-yl] benzenesulfonamide derivatives were synthesised and subjected to cytotoxicity studies against MCF-7 cell lines by Mostafa and Mansour. Compound **6d** was found to be more potent than doxorubicin (Fig. 1b) [15]. 4,6-diaryl-2-imino-1,2-dihydropyridine-3-carbonitriles were synthesized and tested against human HT-29 colon adenocarcinoma tumor cells by A.H. Abadi et al. The IC<sub>50</sub> value for few substituents was found to be 3, 4.17, 12 μM, respectively. Through the molecular docking studies, the cyano and imino group displayed the hydrogen-bonding interaction with the amino acid residues present at the target site. Compound **1d** was found to be most potent (Fig. 1c) [16]. Literature survey indicated that there is still more to explore in this area. Therefore, we sought to develop molecules combining two moieties, i.e., diphenyl ether-bearing hydroxyl group and 3-cyano-2-aminopyridine, in order to develop potential cytotoxic agents targeting hER. Triclosan is reported to adversely affect HepG2 cells by DNA methylation dysregulation, and Diorcinol D (DD), a diphenyl ether derivative, has also shown potent cytotoxicity against A-549 cell lines [8, 17]. Hence, we chose A-549, HepG2 and Vero cells for carrying out the cytotoxicity studies of the synthesized compounds (**3a–q**). In this study, we have carried out computational studies to investigate the binding mode of the molecules with the receptor. For this purpose, we have docked the synthesized compounds with the crystal structure of human enoyl-acyl carrier protein reductase (PDB 4W82) obtained from the protein data bank [18]. Computational studies were carried out using Schrodinger suite 2017-4. The present work is a preliminary work involving computational study, and in vitro enzyme inhibition studies have not been performed to support the work.

## Results and discussion

### Synthesis and spectral analysis

Scheme (Fig. 2) outlines the synthesis of the target compounds **3a–q**. Initially, vanillin was condensed with phenyl boronic acid to obtain 3-methoxy-4-phenoxybenzaldehyde (1). The aldehyde (**1**) obtained was demethylated by treating with HBr giving 3-hydroxy-4-phenoxybenzaldehyde (**2**) [19]. Compounds **3a–q** were synthesized by the reaction of aldehyde (**2**), aryl ketones, malononitrile and ammonium acetate in dioxane. The reported mechanism involved in this synthesis initially involves the formation of enamine derivative obtained by reaction of ketone with ammonium acetate and formation of alkylidene malononitrile obtained by reaction of aldehyde (**2**) with malononitrile. Further, the reaction of enamine derivative with alkylidene malononitrile results in the formation of the Michael adduct. The intermediate

<sup>2</sup> Department of Pharmaceutical Biotechnology, Manipal College of Pharmaceutical Sciences, Manipal Academy of Higher Education, Manipal 576 104, India

<sup>3</sup> Department of Microbiology, Melaka Manipal Medical College, Manipal Academy of Higher Education, Manipal 576104, India

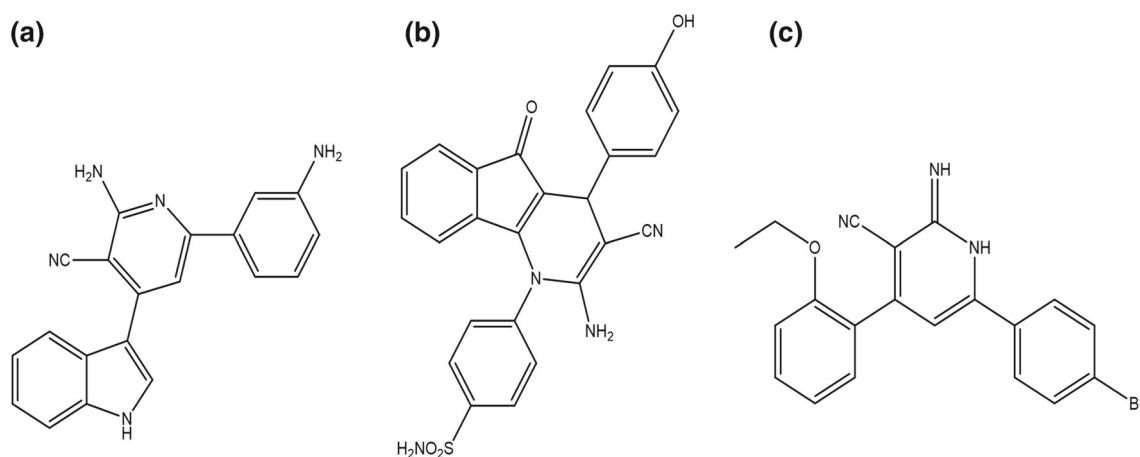
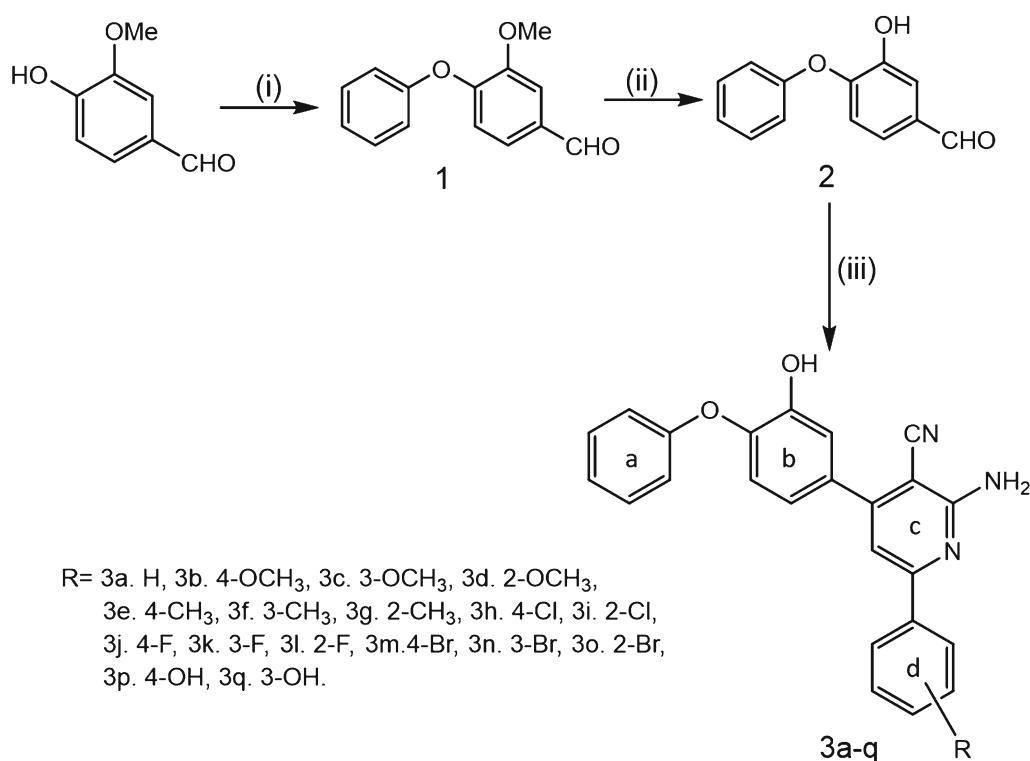


**Fig. 1** 2-Amino-3-cyanopyridine-related analogues



**Reagents and conditions:** (i) PhB(OH)<sub>2</sub>, Cu(OAc)<sub>2</sub>, C<sub>5</sub>H<sub>5</sub>N, CH<sub>2</sub>Cl<sub>2</sub>, 25–27°C, 72h;  
 (ii) HBr(48%v/v), GlacOH, 110–112°C, 24h; (iii) ArCOCH<sub>3</sub>, NH<sub>4</sub>OAc, CH<sub>2</sub>(CN)<sub>2</sub>, 1,4-Dioxane, reflux,  
 101°C, 24h.

**Fig. 2** Scheme

formed undergoes cycloaddition, isomerization and aromatization to get the desired compounds [20, 21]. Various electron-donating/-withdrawing groups were substituted at the D ring in order to understand the influence of various groups and their position on the anticancer activity. The IR spectra of the synthesized compounds indicated characteristic C≡N peak around 2210–2220 cm<sup>-1</sup> and NH<sub>2</sub> asymmetric

and symmetric stretch between 3300 and 3500 cm<sup>-1</sup> and a broad peak above 3300 cm<sup>-1</sup>, indicating the presence of hydroxyl group. <sup>1</sup>H NMR spectra of all the synthesized compounds showed OH proton as singlet around δ 9.5–10.0 ppm. Aromatic protons and NH<sub>2</sub> group were seen as a multiplet around δ 8.0–6.5 ppm [21]. The <sup>13</sup>C NMR of the synthesized compounds showed a signal at 109 ppm due to

C≡N group. Signals due to phenyl group were found in 116–149.65 ppm range. The signal at 165 was attributed to C–NH<sub>2</sub> of the pyridine ring. <sup>1</sup>H NMR spectra for the compound **3p** showed multiplet between 8.02 and 6.83 ppm corresponding to 13 aromatic protons and two NH<sub>2</sub> group protons and a singlet for two protons of hydroxyl group at ring B and ring D at 9.95 ppm. <sup>13</sup>C NMR spectra for the same compound displayed chemical shift at 161.33 ppm (C–NH<sub>2</sub> of the pyridine ring), 160.04 ppm (C–OH of the D ring), 159.05 ppm (C–O of A ring), 157.86 ppm, 117.84 ppm, 154.44 ppm (C of pyridine ring), 149.58 ppm (C–OH of B ring), 144.53 ppm (C–O of B ring), 130.23 ppm (two equivalent carbon of D ring), 129.41 ppm (two equivalent carbon of A ring), 128.80 ppm (C of D ring), 122.98 ppm (C of A ring), 134.50 ppm, 121.87 ppm, 120.25 ppm, 117.54 ppm (C of B ring), 117.28 ppm (two equivalent carbon of A ring), 115.89 ppm (two equivalent carbon of A ring), 108.48 ppm (CN group) and 85.53 ppm (C–CN of pyridine ring). <sup>1</sup>H NMR spectra for the compound **3b** showed multiplet between 8.13 and 6.62 ppm corresponding to 13 aromatic protons and two NH<sub>2</sub> group protons and a singlet for proton of hydroxyl group at ring B (9.952 ppm) and a singlet for three protons of methoxy group at 3.87 ppm. <sup>13</sup>C NMR spectra for the same compound displayed chemical shift at 161.36 ppm (C–NH<sub>2</sub> of the pyridine ring), 161.3 ppm (C–OCH<sub>3</sub> of the D ring), 158.68 ppm (C–O of A ring), 157.84 ppm, 154.59 ppm, 117.56 ppm (C of pyridine ring), 149.56 ppm (C–OH of B ring), 144.58 ppm (C–O of B ring), 134.39 ppm (C of B ring), 130.35 ppm (C of D ring), 129.41 ppm (two equivalent carbon of A ring), 128.80 ppm (C of D ring), 122.99 ppm (C of A ring), 121.84 ppm, 117.72 ppm (C of B ring), 120.28 ppm (two equivalent carbon of D ring), 117.30 ppm (two equivalent carbon of A ring), 114.49 ppm (two equivalent carbon of D ring), 108.74 ppm (CN group), 85.95 ppm (C–CN of pyridine ring) and 55.79 ppm (OCH<sub>3</sub> group).

### Cell viability study by MTT assay

MTT cell viability assay which involves the action of mitochondrial dehydrogenase on MTT to produce dark-blue formazan from MTT (3-(4,5-dimethylthiazol-2-yl)-2,5-diphenyltetrazolium bromide) was used to evaluate the anticancer activity of the synthesized compounds [22]. Synthesized compounds **3a–q** were evaluated for cell toxicity activity against A-549, HepG2, and normal kidney epithelial cells (Vero) using MTT assay. Compounds **3b** (IC<sub>50</sub> of 16.74 ± 0.45 μM) and **3p** (IC<sub>50</sub> of 10.57 ± 0.54 μM) were found to be the most active against A-549 cell line and were chosen for further studies. Eleven compounds showed moderate cytotoxicity (IC<sub>50</sub> between 20 μM–40 μM). The positive control cisplatin showed cytotoxicity at IC<sub>50</sub> of 33.99 ± 0.90 μM, whereas triclosan exhibited cytotoxicity at 23.96 ± 0.70 μM. Remaining four compounds were not

**Table 1** Effect of synthetic compounds treatment on proliferation of A-549 and HepG2 cells after 48 h and Vero cells after 72 h

Entry	Compound	IC <sub>50</sub> (μM)*		
		A-549	HepG2	Vero
1.	<b>3a</b>	38.25 ± 0.23	>100	>100
2.	<b>3b</b>	16.74 ± 0.45	>100	>100
3.	<b>3c</b>	34.22 ± 0.62	>100	>100
4.	<b>3d</b>	29.33 ± 0.13	>100	>100
5.	<b>3e</b>	36.46 ± 0.54	>100	>100
6.	<b>3f</b>	41.47 ± 0.24	>100	>100
7.	<b>3g</b>	35.62 ± 0.60	>100	>100
8.	<b>3h</b>	22.46 ± 0.90	>100	>100
9.	<b>3i</b>	27.43 ± 1.20	>100	>100
10.	<b>3j</b>	36.09 ± 0.00	>100	>100
11.	<b>3k</b>	60.45 ± 0.35	>100	>100
12.	<b>3l</b>	38.41 ± 0.43	>100	>100
13.	<b>3m</b>	22.11 ± 0.30	>100	>100
14.	<b>3n</b>	33.29 ± 0.88	>100	>100
15.	<b>3o</b>	44.43 ± 0.30	>100	>100
16.	<b>3p</b>	10.57 ± 0.54	>100	>100
17.	<b>3q</b>	25.316 ± 0.51	>100	>100
18.	Triclosan	23.96 ± 0.70	>100	>100
19.	Cisplatin	33.99 ± 0.90	>100	>100

\*Data presented as mean ± SEM, *N* = 3

significantly cytotoxic (IC<sub>50</sub> above 40 μM). Almost all the compounds showed good selectivity to screened cell lines over normal kidney epithelial cells (Vero). The compounds were found to be safe with IC<sub>50</sub> value > 100 μM. Compounds did not exhibit any notable cytotoxicity against HepG2 cell line [IC<sub>50</sub> above > 100 μM] (Table 1). Among the tested compounds, substitutions at the D ring of the test molecules resulted in enhanced anticancer activity in comparison with substitutions at meta- and ortho-position. Among the para substituents, methoxy group substitution and hydroxyl group substitution at para position of the phenyl ring were found to be most active.

### AO/EB nuclear staining

Apoptosis is the programmed cell death phenomenon leading to characteristic morphological changes in the cell [23]. Cell staining with fluorescent acridine orange and ethidium orange is a very common and precise method to detect, classify apoptosis and differentiate it from necrosis [24]. Based on the IC<sub>50</sub> values of **3b** and **3p** in A-549, these compounds were selected for AO/EB nuclear staining method. The cell line was treated with the synthesized compounds, incubated for 48 h, stained with AO/EB dye and was observed under a fluorescent microscope to visualize the changes in the mor-

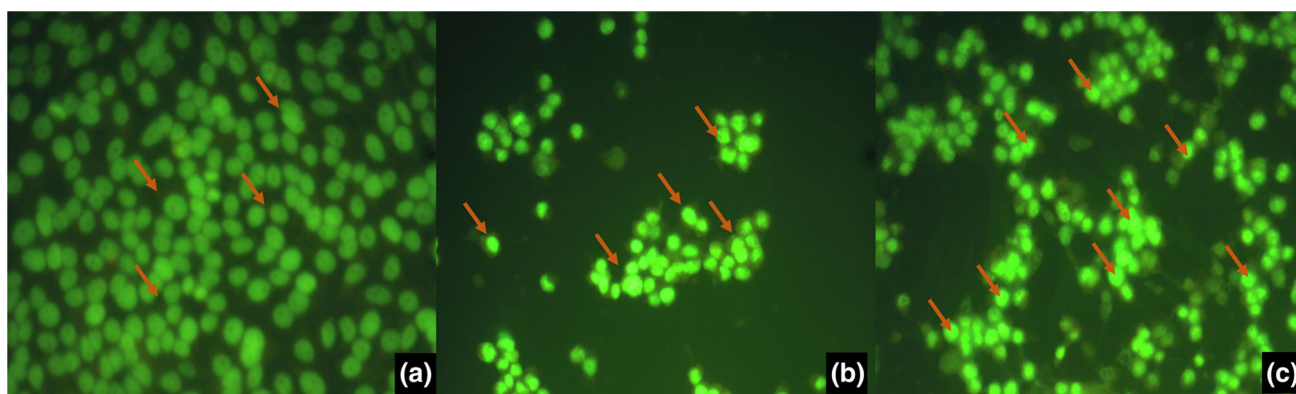


**Fig. 3** Apoptosis induction by AO/EB stain after 48 h in A-549 cells: **a** normal control, **b** compound **3b**, **c** compound **3p**

phology of the cell nucleus (Fig. 3). From Fig. 3a, it is evident that untreated normal control A-549 cells showed normal green integral nuclei depicting normal cell morphology. A-549 cells treated with **3b** and **3p** (Fig. 3b, c) showed fluorescent green nuclei, condensed chromatin and smaller diameter indicating initial apoptosis when observed under a fluorescence microscope. Further, compounds **3b** and **3p** were taken up for DNA fragmentation study.

### DNA fragmentation assay

Nuclear DNA fragmentation is considered as one of the biochemical hallmarks of apoptosis showing distinct DNA ladder fragments of 180–200 base pairs and multiples on agarose gel, whereas cell necrosis results in production of diffused smear of DNA on electrophoresis [25]. DNA laddering assay was performed to ensure that the cell death of A-549 cells when exposed to the synthesized compounds (**3b**, **3p**, TCL and cisplatin) occurred due to apoptosis. DNA fragmentation pattern was obtained for control cells and the treated cells at their  $IC_{50}$  value concentration by agarose gel electrophoresis method (Fig. 4). After 4 h of treatment of A-549 cells with **3b**, TCL and cisplatin, a distinct ladder was seen (Fig. 4, lane 2–4) and untreated control did not show any DNA ladder (Fig. 4, lane 5). For compound **3p** (Fig. 4, lane 1), characteristic DNA ladder was not seen. The results obtained showed the cleavage of chromosomal DNA into nucleosomal unit, thus confirming cell cytotoxicity [26] by the compound (**3b**) due to apoptosis. For compound **3p**, characteristic DNA fragmentation was not seen, thus indicating the possibility of cell toxicity through necrosis.

### Cell cycle analysis

The cell distribution in various phases of its growth progression cycle depends on the underlying mechanism for the cytotoxicity produced by the synthesized compounds [26, 27]. Based on the DNA fragmentation studies, flow cytome-

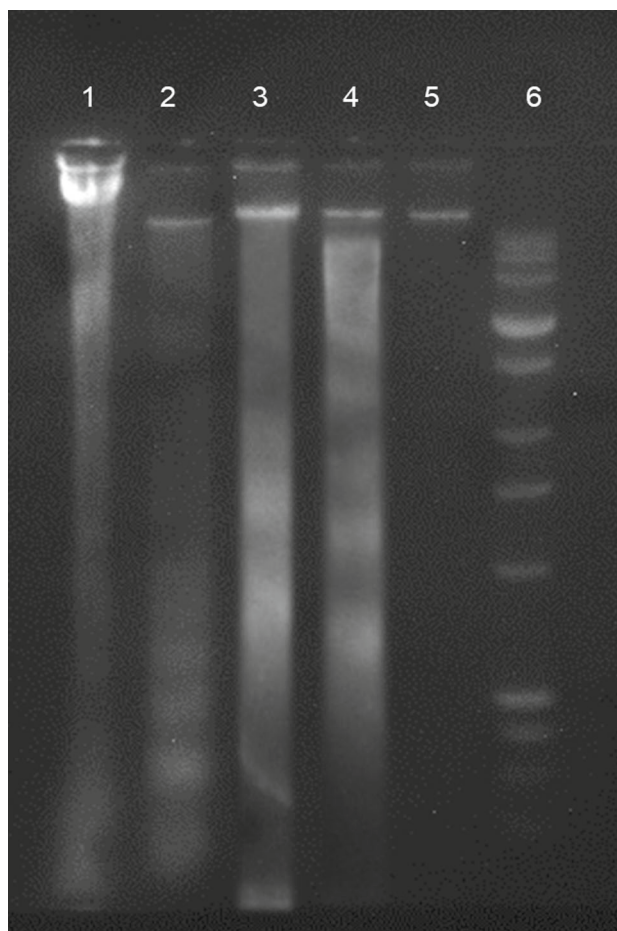


**Fig. 4** DNA fragmentation studies by agarose gel electrophoresis (1.5%); lane 1: A-549 cells + **3p**; lane 2: A-549 cells + **3b**; lane 3: A-549 cells + TCL; lane 4: A-549 cells + cisplatin; lane 5: A-549 cells + control; lane 6: DNA ladder

try study was done to understand the underlying mechanism of the cell inhibition by the compounds **3b** and TCL (Fig. 5). The results were obtained as % cells distribution in G<sub>0</sub>/G<sub>1</sub>, S, and G<sub>2</sub>/M phase. The untreated cells (control) exhibited the

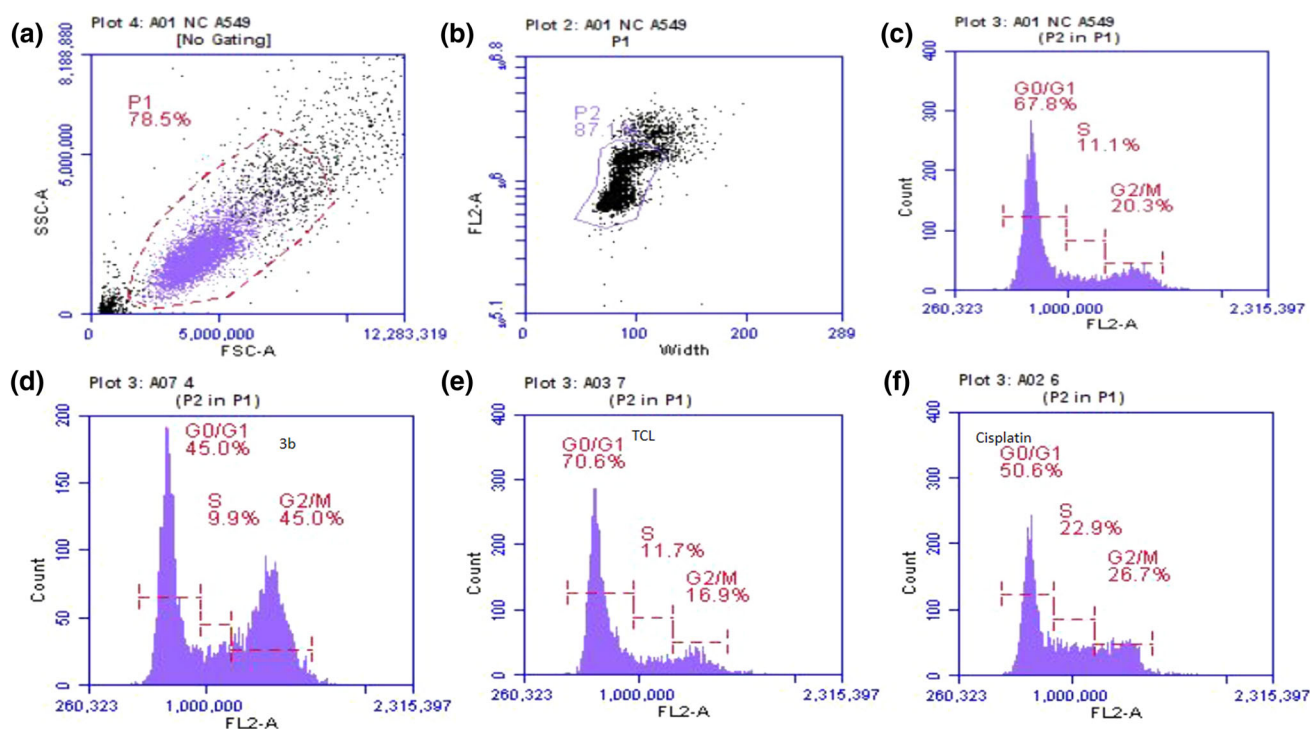


**Fig. 5** Cell cycle phase distribution of A-549 cells after 48 h treatment; the % cells enrichment specifically in G0/G1, S, and G2/M phase was assessed by flow cytometry; **a** FSC A versus SSC plot for normal control cells; **b** width versus FL2-A plot for 2n to 4n normal control gated cells;

(c) FL2-A versus count histogram plot for normal control (0.01%); (d, e and f) FL2-A versus count histogram plots for **3b**, TCL and cisplatin, respectively. FSC forward scatter, SSC side scatter; TCL triclosan

cell enrichment of 67.8% in G0/G1, 11.1% in S and 20.3% in G2/M phase, whereas in cisplatin-treated cells, the percentage of cells in S phase and G2/M phase was 22.9% and 26.7%, respectively, indicating cell cycle arrest. As mentioned in earlier studies, TCL ( $IC_{50}$   $23.96 \pm 0.7 \mu\text{M}$ )-treated A-549 cells exhibited 70.6% of accumulation in G0/G1 phase. In comparison with cisplatin and TCL, significant increase in the cell count was found in G2/M phase (45.0%) and a reduction of cell count was found in S phase and G0/G1 phase when treated with **3b** ( $IC_{50}$   $16.74 \pm 0.45 \mu\text{M}$ ). Therefore, it may be attributed that compound **3b** produced cytotoxicity due to cell cycle arrest at G2/M phase. The mechanism for cell growth inhibition by compound **3b** was found to be different when compared to the triclosan through this study.

### Molecular docking studies

The in silico computational method is very useful to determine the types of interactions between the compounds and the target receptor. All the synthesized compounds were docked with 4W82 protein by using grid-based method. Site map tool was used to determine the best binding site for the ligands on the protein. A total of five sites were identified by the site map. Site 1 was selected as the best binding site

based on its site score (1.076) and site volume ( $569.037 \text{ \AA}^3$ ) (supplementary data) with active residues. A grid was generated at site 1. After the grid was generated, the prepared ligands were docked with the target active site using Glide Xtra precision (XP) mode. Thirteen molecules showed dock score above  $-7.00$  kcal/mol when compared to triclosan (dock score of  $-6.13$  kcal/mol). Compound **3b** showed dock score of  $-7.098$  kcal/mol and **3p** of  $-7.85$  kcal/mol. The ligands showed H-bond interactions with amino acid residues Glycine 1679, Asparagine 1572, Glycine 1846, and few ligands showed  $\pi$  cation interaction with Lysine 1771 of the protein 4W82 (supplementary data). Compound **3b** showed dock score above  $-7.0$  kcal/mol and displayed one hydrogen bond interaction between OH group on the diphenyl ether ring and Asparagine 1572, second hydrogen bond interaction between  $\text{NH}_2$  group and Glycine 1846 and third hydrogen bond interaction between CN group and Glycine 1679. The  $\pi$  cation interaction was found between A ring of diphenyl ether moiety and Lysine 1771 (Fig. 6). Compound **3p** exhibited maximum four hydrogen bonds interactions involving OH group at D ring with Alanine 1844,  $\text{NH}_2$  group with Glycine 1846, CN group with Glycine 1679 and OH group at the diphenyl ether moiety with Asparagine 1572 (Fig. 7). Triclosan showed one H-bond interaction with

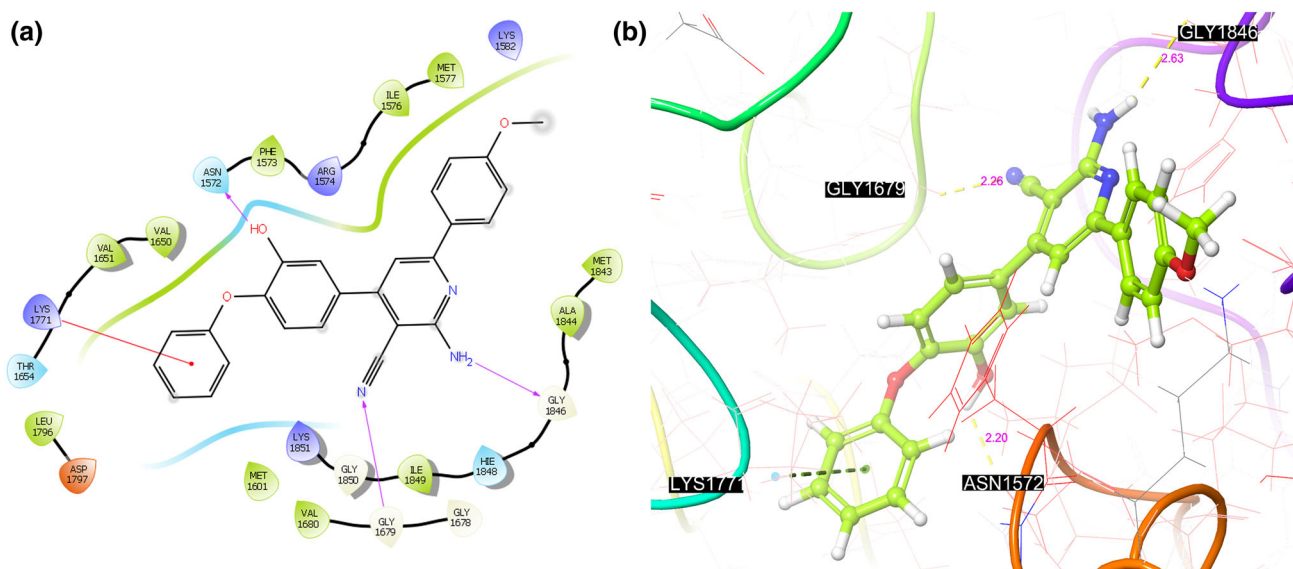


**Fig. 6** **a** Graphical illustration of predicted binding mode in the active site of 4W82 for compound **3b**. The hydrogen bond interactions are represented by magenta arrow, and  $\pi$  cation interactions are represented

by red bond, **b** 3D interaction between human enoyl-acyl carrier protein reductase (PDB: 4W82) and compound **3b**

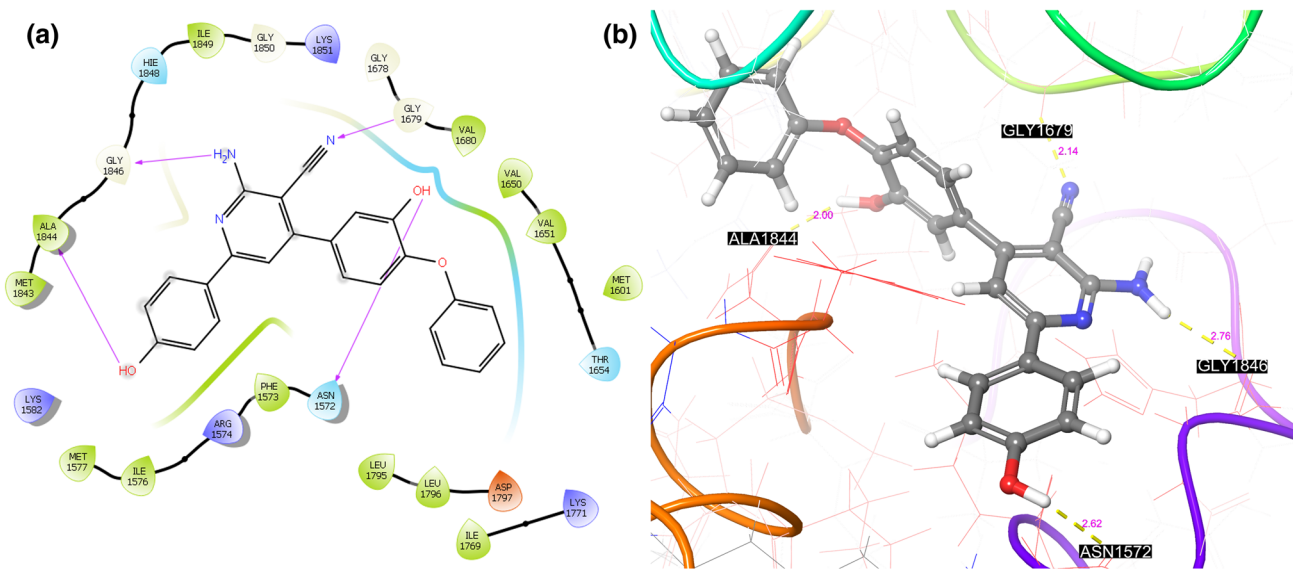


**Fig. 7** **a** Graphical illustration of predicted binding mode in the active site of 4W82 for compound **3p**. The hydrogen bond interactions are represented by magenta arrow; **b** 3D interaction between human enoyl-acyl carrier protein reductase (PDB: 4W82) and compound **3p**

Phenylalanine 1573 (Fig. 8). More number of interactions particularly H-bond between ligand and receptor along with dock score contributes toward its strong affinity toward the receptor [28] which may be responsible for the potent activity of compounds **3b** and **3p**. This was further confirmed through MMGBSA. The binding energy between receptor and ligand is dependent on H-bond strength and  $\pi$  cation interactions. The negative  $dG$  values correspond to stable ligand–receptor complex and thermodynamic practicability

of binding [29]. The results (Table 2) show that compounds **3b**, **3h**, **3m**, **3p** and **3q** showed binding energies more than  $-56.500$  kcal/mol which is appreciable score depicting the strong affinity of the ligands toward the receptor. Thus, more number of interaction between ligand and receptor, better binding energy, better glide score and thermodynamically stable ligand–receptor complex of synthesized compounds **3p** and **3b** would have contributed towards the potent anticancer activity when compared to triclosan.

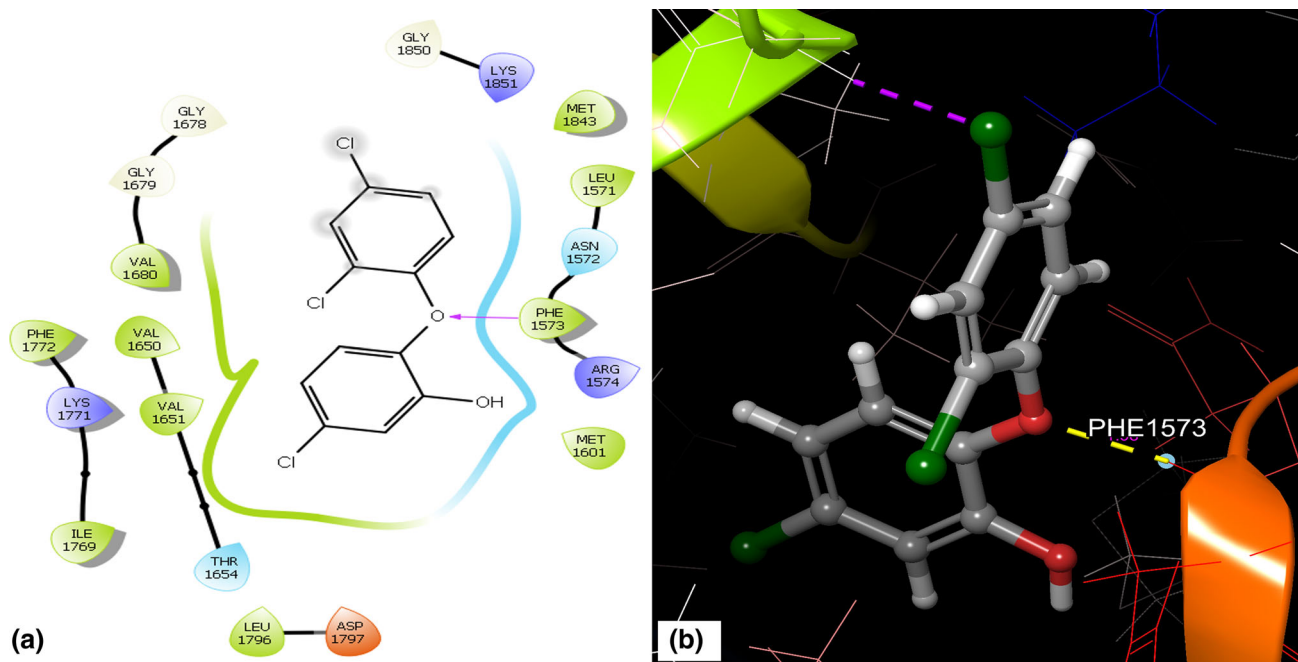


**Fig. 8** **a** Graphical illustration of predicted binding mode in the active site of 4W82 for triclosan. The hydrogen bond interactions are represented by magenta arrow; **b** 3D interaction between human enoyl-acyl carrier protein reductase (PDB: 4W82) and triclosan

## Drug-likeness property

The results obtained through QikProp tool (Table 3) show all the ligands following Lipinski's rule of five; i.e., drug-gable molecule has  $\log P \leq 5$ , molecular weight  $< 500$  g/mol, hydrogen bond acceptors  $\leq 10$ , hydrogen bond donors  $\leq 5$  and molar refractivity between 40 and 130. No ligand was found to violate the Lipinski's rule of five [29].

## Conclusion

The synthesis of novel diphenyl ether analogues **3a–q** has been reported in the present research work showing anticancer activity against cancer cell lines. Compounds **3b** ( $IC_{50}$  value  $16.74 \pm 0.45$ ) and **3p** ( $IC_{50}$  value  $10.57 \pm 0.54$   $\mu$ M) inhibited A-549 cells more effectively in comparison with the other synthesized compounds. Compound **3b** (para-methoxy substituted) showed cell toxicity in A-549 cells due to apoptosis. This compound can serve as a promising lead for the development of new anticancer drugs. It was found that TCL arrested cell cycle growth at G0/G1 phase, whereas compound **3b** showed tremendous increase in the cells at G2/M phase. In silico studies depicted good docking score of the compounds **3b** and **3p** with the receptor 4W82, strong affinity toward receptor target through H-bond interaction and binding energy score in comparison with triclosan. Detailed study is required to study the proper mechanism of cell growth inhibition in A549 cells by these compounds. Further exper-

iments would assist in structure modifications to increase the anticancer activity of this scaffold. Hence, it could be interpreted that **3b** compound-treated cells could produce damage to the cancerous A549 cells, signifying the substantial potential of this compound in the treatment of lung cancer.

## Experimental

### Materials and methods

#### Reagents and chemicals

The chemicals and solvents used in synthesis and cell line studies were purchased commercially. Melting points were obtained in open capillary tubes and are uncorrected. The  $^1H$  NMR and  $^{13}C$  NMR spectra were obtained on NMR spectrometer (AV400—400 MHz high-resolution multinuclear FT-NMR spectrometer, Bruker, USA). Mass spectroscopy was performed on LC–MS (linear ion trap, APCI mode, LC/MS, Thermo Fisher Scientific LTQ21532 series, USA) and GC–MS (GCMS-QP5050A, Shimadzu, Japan).

Three cell lines such as HepG2 (human hepatocellular carcinoma cell line), A-549 (adenocarcinomic human alveolar basal epithelial cells), Vero (normal African green monkey kidney epithelial cells) used in this study were obtained from the National Center for Cell Science, Pune, India, and maintained in tissue and cell culture in high glucose DMEM medium with 10% FBS and 1% antibiotic–antimy-

**Table 2** Binding energy calculation of the (4W82-ligands) docked complexes

Compound	XP glide score	Prime MMGBSA dG bind (k cal/mol)	MMGBSA dG bind coulomb (k cal/mol)	MMGBSA dG bind covalent (k cal/mol)	MMGBSA dG bind vdW (k cal/mol)	MMGBSA dG bind Solv GB (k cal/mol)
<b>3a</b>	-8.001	-54.079	-11.037	1.702	-50.724	33.529
<b>3b</b>	-7.098	-56.634	-13.559	2.543	-53.436	36.338
<b>3c</b>	-7.63	-54.571	-9.335	0.817	-50.325	31.792
<b>3d</b>	-7.513	-53.833	-10.758	0.322	-51.379	35.555
<b>3e</b>	-7.954	-56.472	-11.243	1.752	-52.779	34.260
<b>3f</b>	-6.785	-55.037	-11.324	1.875	-52.160	34.498
<b>3g</b>	-6.008	-53.798	-10.669	1.860	-50.214	32.792
<b>3h</b>	-7.5	-58.924	-11.019	1.611	-53.182	32.230
<b>3i</b>	-7.686	-54.571	-9.335	0.817	-50.325	31.792
<b>3j</b>	-7.712	-56.055	-10.748	1.806	-51.460	32.018
<b>3k</b>	-6.563	-53.670	-7.282	2.011	-51.228	30.162
<b>3l</b>	-7.839	-54.199	-9.721	0.773	-50.013	32.199
<b>3m</b>	-7.541	-57.515	-10.955	1.577	-53.853	33.220
<b>3n</b>	-5.446	-53.798	-10.669	1.860	-51.622	32.625
<b>3o</b>	-7.764	-55.296	-15.619	1.754	-52.026	35.217
<b>3p</b>	-7.851	-57.314	-19.482	2.594	-50.591	37.800
<b>3q</b>	-8.418	-57.769	-18.812	4.210	-49.603	34.355
Triclosan	-6.13	-43.275	-12.089	1.529	-33.548	18.199

**Table 3** Drug-likeness properties of the compounds as per the QikProp software application

Compd.	MW	Hd <sup>a</sup>	Hb <sup>b</sup>	PSA <sup>c</sup>	QPlogPo/w <sup>d</sup>	Rule of five <sup>e</sup>	Oral abs (%)
<b>3a</b>	379	3.0	4.25	98.7	4.091	0	92.723
<b>3b</b>	409	3.0	5.0	98.6	4.221	0	94.094
<b>3c</b>	409	3.0	5.0	96.4	4.208	0	93.817
<b>3d</b>	409	3.0	5.0	90.41	4.243	0	93.529
<b>3e</b>	393	3.0	4.25	90.4	4.386	0	94.525
<b>3f</b>	393	3.0	4.25	88.5	4.41	0	95.021
<b>3g</b>	393	3.0	4.25	90.37	4.418	0	96.873
<b>3h</b>	414	3.0	4.25	90.37	4.574	0	95.604
<b>3i</b>	414	3.0	4.25	90.37	4.462	0	96.01
<b>3j</b>	397	3.0	4.25	90.42	4.317	0	94.099
<b>3k</b>	397	3.0	4.25	90.62	4.336	0	94.612
3 l	397	3.0	4.25	90.42	4.256	0	93.661
3 m	458	3.0	4.25	90.43	4.647	0	96.029
<b>3n</b>	458	3.0	4.25	91.04	4.668	0	96.553
<b>3o</b>	458	3.0	4.25	112.92	4.495	0	94.907
<b>3p</b>	395	4.0	5.0	112.97	3.298	0	78.859
<b>3q</b>	395	4.0	5.0	110.63	3.308	0	79.133
Triclosan	290	1.0	1.25	28.76	4.75	0	100

<sup>a</sup>Hd hydrogen bond donor<sup>b</sup>Hb hydrogen bond acceptor<sup>c</sup>PSA polar surface area<sup>d</sup>QPlogPo/w = LogP in o/w<sup>e</sup>Rule of 5 = Lipinski's rule of five: 1 = violation, 0 = within the limit<sup>f</sup>Human oral absorption (%)

cotic solution, at 37 °C in an CO<sub>2</sub> incubator under 5% CO<sub>2</sub> and 95% air-humidified condition (CLS-170-B-8, Serial No. 201020569, Esco Micro Pte. Ltd.).

## Synthesis

**3-methoxy-4-phenoxybenzaldehyde**, **1** Vanillin (32.89 mmol) was stirred in anhydrous dichloromethane (60 mL) at 25–27 °C. Then, activated molecular sieves (4 Å, 2.5 g), phenyl boronic acid (49.33 mmol), copper (II) acetate (40.58 mmol) and anhydrous pyridine (64.78 mmol, 5.28 mL) were added sequentially. The progress of the reaction was checked by TLC (hexane/ethyl acetate; 8:2). After the completion of the reaction (72 h), the reaction mixture was filtered under vacuum. Further washing of filtrate was done using a dilute aqueous hydrochloric acid solution (2 M, 50 mL), dried over anhydrous MgSO<sub>4</sub> and evaporated under vacuum till dryness [19]. The purification of the crude product was done using column chromatography on silica 100–200 using hexane: ethyl acetate (8:2) to achieve the desired compound. Yield = 5 g (67%); mp = 40–42 °C;  $R_f$  = 0.83 (hexane: ethyl acetate = 8:2);  $\lambda_{\max}$  = 275.2 nm (MeOH).

**3-hydroxy-4-phenoxybenzaldehyde**, **2** 3-Methoxy-4-phenoxybenzaldehyde (**1**) (3 g, 13.15 mmol) was stirred in glacial AcOH (50 mL), and HBr (48% v/v, 12 mL) was added. Resulting reaction mixture was refluxed at 112–115 °C. The reaction progress was monitored by TLC (hexane/ethyl acetate; 8:2). At the end of 14 h, the reaction mixture was cooled to room temperature and was poured into 50 mL of ice-cold water with continuous stirring. The product was extracted using ethyl acetate (3 × 50 mL). The ethyl acetate layers were combined and rinsed with saturated NaHCO<sub>3</sub> solution. Ethyl acetate layer was dried over anhydrous MgSO<sub>4</sub>, and the ethyl acetate was evaporated under vacuum [19]. The crude product was purified by column chromatography on silica 100–200 using hexane: ethyl acetate (8:2) system to achieve the corresponding off-white crystalline solid compound.

Yield = 1.6 g (60%); mp = 72–74 °C;  $R_f$  = 0.59 (hexane:ethyl acetate = 6:4);  $\lambda_{\max}$  = 275 nm (MeOH); IR (KBr, cm<sup>-1</sup>) = 3452, 3057, 1680, 1527, 1483, 1440, 1245, 1132; <sup>1</sup>H NMR (400 MHz, DMSO-*d*<sub>6</sub>):  $\delta$  10.08 (s, 1H, OH), 9.85 (s, 1H, CHO), 7.42 (d,  $J$  = 1.6 Hz, 1H, Ar-H), 7.39–7.35 (m, 3H, Ar-H), 7.14–7.10 (m, 1H, Ar-H), 7.01–7.26 (d,  $J$  = 8 Hz, 1H, Ar-H), 6.98–6.96 (td,  $J$  = 8 Hz and 1.6 Hz, 2H, Ar-H); LCMS (+ESI, m/z): 215.069 (M+H)<sup>+</sup>.

### General procedure for the preparation of compounds, 3a–q

**Synthesis of 2-amino-4-(3-hydroxy-4-phenoxyphenyl)-6-phenylnicotinonitrile**, **3a** A solution of 3-hydroxy-

4-phenoxybenzaldehyde (**2**) (2.3 mmol), acetophenone (2.3 mmol), ammonium acetate (1.5 g, 19.4 mmol) and malononitrile (0.253 mL, 2.3 mmol) in dioxane (5.0 mL) was refluxed with stirring for 24 h. Dioxane was evaporated under vacuum, and the reaction mixture was poured into water (30 mL) and the product was extracted with ethyl acetate [20, 21]. The ethyl acetate layer was separated, dried over anhydrous MgSO<sub>4</sub> and evaporated under reduced pressure. The crude mixture was purified by column chromatography (hexane: ethyl acetate; 8:2) to get the desired compound.

Yield = 0.46 g (53%); mp = 168–169 °C;  $R_f$  = 0.78 (hexane: ethyl acetate = 8:2); IR (KBr, cm<sup>-1</sup>) = 3479 and 3360 (asym. and sym. stretching of –NH<sub>2</sub>), 3068 (Ar-H), 2214 (C≡N stretching); <sup>1</sup>H NMR (400 MHz, DMSO-*d*<sub>6</sub>)  $\delta$  9.97 (s, 1H, OH), 8.17–6.78 (m, 16H, Ar-H+NH<sub>2</sub>); <sup>13</sup>C NMR (101 MHz, DMSO)  $\delta$  161.39, 159.01, 157.81, 154.83, 149.57, 144.68, 138.01, 134.22, 130.58, 130.23, 130.08, 129.13, 127.69, 123.02, 121.83, 120.33, 117.59, 117.33, 109.54, 86.89; LCMS(+APCI, m/z): 380 (M+H)<sup>+</sup>.

**2-amino-4-(3-hydroxy-4-phenoxyphenyl)-6-(4-methoxyphenyl) nicotinonitrile (3b)** Yield = 0.53 g (46%); mp = 178–179 °C;  $R_f$  = 0.74 (hexane: ethyl acetate = 8:2); IR (KBr, cm<sup>-1</sup>) = 3415 and 3360 (asym. and sym. stretching of –NH<sub>2</sub>), 3072 (Ar-H), 2212 (C≡N stretching); <sup>1</sup>H NMR (400 MHz, DMSO-*d*<sub>6</sub>)  $\delta$  9.952 (s, 1H, OH), 8.13–6.92 (m, 15H, Ar-H+NH<sub>2</sub>), 3.87 (s, 3H, OCH<sub>3</sub>); <sup>13</sup>C NMR (101 MHz, DMSO)  $\delta$  161.47, 161.32, 158.68, 157.84, 154.59, 149.56, 144.58, 134.39, 130.35, 130.22, 129.29, 122.99, 121.84, 120.28, 117.72, 117.56, 117.30, 114.49, 108.74, 85.95, 55.79; LCMS(+APCI, m/z): 410 (M+H)<sup>+</sup>.

**2-amino-4-(3-hydroxy-4-phenoxyphenyl)-6-(3-methoxyphenyl) nicotinonitrile (3c)** Yield = 0.44 g (50%); mp = 201–202 °C;  $R_f$  = 0.73 (hexane: ethyl acetate = 8:2); IR (KBr, cm<sup>-1</sup>) = 3473 and 3332 (asym. and sym. stretching of –NH<sub>2</sub>), 3066 (Ar-H), 2220 (C≡N stretching); <sup>1</sup>H NMR (400 MHz, DMSO-*d*<sub>6</sub>)  $\delta$  9.95 (s, 1H, OH), 7.75–6.92 (m, 15H, Ar-H+NH<sub>2</sub>), 3.87–3.81 (s, 3H, OCH<sub>3</sub>); <sup>13</sup>C NMR (101 MHz, DMSO)  $\delta$  161.31, 160.07, 158.81, 157.83, 154.85, 149.57, 144.68, 139.56, 134.22, 130.23, 123.02, 121.83, 120.37, 120.11, 117.64, 117.54, 117.34, 116.34, 114.24, 112.92, 109.74, 87.06, 55.75; LCMS(+APCI, m/z): 410 (M+H)<sup>+</sup>.

**2-amino-4-(3-hydroxy-4-phenoxyphenyl)-6-(2-methoxyphenyl) nicotinonitrile (3d)** Yield = 0.39 g (45%); mp = 214–215 °C;  $R_f$  = 0.71 (hexane: ethyl acetate = 8:2); IR (KBr, cm<sup>-1</sup>) = 3446 and 3350 (asym. and sym. stretching of –NH<sub>2</sub>), 3242 (Ar-H), 2210 (C≡N stretching); <sup>1</sup>H NMR (400 MHz, DMSO-*d*<sub>6</sub>)  $\delta$  9.987 (s, 1H, OH), 7.80–6.96 (m, 15H, Ar-H+NH<sub>2</sub>), 3.843 (s, 3H, OCH<sub>3</sub>); <sup>13</sup>C NMR (101 MHz, DMSO)  $\delta$  161.35, 158.41, 157.73, 157.62,

153.39, 149.60, 144.70, 134.24, 131.47, 131.20, 130.25, 127.68, 123.06, 121.80, 120.94, 120.14, 117.59, 117.44, 117.39, 114.04, 112.54, 86.24, 56.20; LCMS(+APCI, m/z): 410 (M+H)<sup>+</sup>.

**2-amino-4-(3-hydroxy-4-phenoxyphenyl)-6-(p-tolyl)**

**nicotinonitrile (3e)** Yield=0.57 g (65%); mp=174–175 °C;  $R_f$  = 0.77 (hexane: ethyl acetate = 8:2); IR (KBr, cm<sup>-1</sup>) = 3495 and 3358 (asym. and sym. stretching of -NH<sub>2</sub>), 3037(Ar-H), 2218 (C≡N stretching); <sup>1</sup>H NMR (400 MHz, DMSO-*d*<sub>6</sub>) δ 9.96 (s, 1H, OH), 8.05–6.97 (m, 15H, Ar-H+NH<sub>2</sub>), 2.38 (s, 3H); <sup>13</sup>C NMR (101 MHz, DMSO) δ 161.36, 158.97, 157.83, 154.71, 149.57, 144.62, 140.39, 135.22, 134.30, 130.22, 129.74, 127.63, 123.00, 121.85, 120.30, 117.61, 117.57, 117.30, 109.19, 86.52, 21.38; LCMS(+APCI, m/z): 394 (M+H)<sup>+</sup>.

**2-amino-4-(3-hydroxy-4-phenoxyphenyl)-6-(m-tolyl)nicotinonitrile (3f)**

Yield=0.44 g (50%); mp=199–200 °C;  $R_f$  = 0.76 (hexane: ethyl acetate = 8:2); IR (KBr, cm<sup>-1</sup>) = 3485 and 3365 (asym. and sym. stretching of -NH<sub>2</sub>), 3234, 3059 (Ar-H), 2214 (C≡N stretching); <sup>1</sup>H NMR (400 MHz, DMSO-*d*<sub>6</sub>) δ 10.03 (s, 1H, OH), 8.02–6.98 (m, 15H, Ar-H+NH<sub>2</sub>), 2.45 (s, 3H); <sup>13</sup>C NMR (101 MHz, DMSO) δ 161.31, 157.82, 157.14, 155.13, 149.57, 144.75, 140.29, 134.04, 133.18, 131.28, 130.26, 130.23, 126.65, 123.03, 122.72, 121.82, 120.44, 117.69, 117.37, 117.33, 109.74, 87.58, 21.24.; LCMS(+APCI, m/z): 394 (M+H)<sup>+</sup>.

**2-amino-4-(3-hydroxy-4-phenoxyphenyl)-6-(o-tolyl)nicotinonitrile (3g)**

Yield=0.39 g (45%); mp=209–210 °C;  $R_f$  = 0.74 (hexane: ethyl acetate = 8:2); IR (KBr, cm<sup>-1</sup>) = 3514, 3446 and 3313 (asym. and sym. stretching of -NH<sub>2</sub>), 3089 (Ar-H stretching), 2214 (C≡N stretching); <sup>1</sup>H NMR (400 MHz,

DMSO-*d*<sub>6</sub>) δ 9.96 (s, 1H, OH), 7.49–6.78 (m, 15H, Ar-H+NH<sub>2</sub>), 2.39(s, 3H, CH<sub>3</sub>). <sup>13</sup>C NMR (101 MHz, DMSO) δ 162.58, 161.21, 157.75, 154.05, 149.59, 144.76, 139.67, 133.99, 131.17, 130.23, 129.94, 129.66, 126.23, 123.05, 121.78, 120.27, 117.53, 117.40, 117.37, 113.06, 86.28, 20.72; LCMS(+APCI, m/z): 394 (M+H)<sup>+</sup>.

**2-amino-6-(4-chlorophenyl)-4-(3-hydroxy-4-phenoxyphenyl) nicotinonitrile (3h)**

Yield=0.53 g (60%); mp=154–155 °C;  $R_f$  = 0.79 (hexane: ethyl acetate = 8:2); IR (KBr, cm<sup>-1</sup>) = 3496, 3361 (asym. and sym. stretching of -NH<sub>2</sub>), 3062 (Ar-H), 2218 (C≡N stretching); <sup>1</sup>H NMR (400 MHz, DMSO-*d*<sub>6</sub>) δ 9.97 (s, 1H), 8.23–6.83 (m, 15H, Ar-H+NH<sub>2</sub>). <sup>13</sup>C NMR (101 MHz, DMSO) δ 161.35, 157.81, 157.66, 155.03, 149.58, 144.74, 136.81, 135.42, 134.11, 130.23, 129.47, 129.16, 123.03, 121.83, 120.37, 117.63, 117.46, 117.34, 109.52, 87.24; LCMS (+APCI, m/z): 414 (M+H)<sup>+</sup>.

**2-amino-6-(2-chlorophenyl)-4-(3-hydroxy-4-phenoxyphenyl) nicotinonitrile (3i)**

Yield=0.48 g (55%); mp=179–180 °C;  $R_f$  = 0.78 (hexane: ethyl acetate = 8:2); (MeOH); IR (KBr, cm<sup>-1</sup>) = 3485 and 3388 (asym. and sym. stretching of -NH<sub>2</sub>), 3064 (Ar-H), 2216 (C≡N stretching); <sup>1</sup>H NMR (400 MHz, DMSO-*d*<sub>6</sub>) δ 9.88 (s, 1H, OH), 7.65–6.93 (m, 15H, Ar-H+NH<sub>2</sub>); <sup>13</sup>C NMR (101 MHz, DMSO) δ 161.47, 159.46, 157.70, 153.90, 149.64, 144.89, 138.60, 133.73, 131.74, 131.43, 131.02, 130.42, 130.24, 127.74, 123.08, 121.82, 120.23, 117.47, 117.43, 117.27, 113.57, 87.11.; LCMS(+APCI, m/z): 414 (M+H)<sup>+</sup>.

**2-amino-6-(4-fluorophenyl)-4-(3-hydroxy-4-phenoxyphenyl) nicotinonitrile (3j)**

Yield=0.53 g (60%); mp=152–153 °C;  $R_f$  = 0.75 (hexane: ethyl acetate = 8:2); IR (KBr, cm<sup>-1</sup>) = 3495 and 3358 (asym. and sym. stretching of -NH<sub>2</sub>), 3066 (Ar-H), 2218 (C≡N stretching); <sup>1</sup>H NMR (400 MHz, DMSO-*d*<sub>6</sub>) δ 9.96 (s, 1H, OH), 8.21–6.83 (m, 15H, Ar-H+NH<sub>2</sub>); <sup>13</sup>C NMR (101 MHz, DMSO) δ 165.11, 162.65, 161.33, 157.81, 154.94, 149.57, 144.70, 134.17, 130.23, 130.08, 123.03, 121.82, 120.35, 117.62, 117.33, 116.73, 116.13, 115.91, 109.35, 86.84; LCMS(+APCI, m/z): 398 (M+H)<sup>+</sup>.

**2-amino-6-(3-fluorophenyl)-4-(3-hydroxy-4-phenoxyphenyl) nicotinonitrile (3k)**

Yield=0.44 g (50%); mp=172–173 °C;  $R_f$  = 0.74 (hexane: ethyl acetate = 8:2); IR (KBr, cm<sup>-1</sup>) = 3473 and 3352 (asym. and sym. stretching of -NH<sub>2</sub>), 3076 (Ar-H), 2218 (C≡N stretching); <sup>1</sup>H NMR (400 MHz, DMSO-*d*<sub>6</sub>) δ 9.96 (s, 1H, OH), 8.00–6.96 (m, 15H, Ar-H+NH<sub>2</sub>); <sup>13</sup>C NMR (101 MHz, DMSO) δ 164.22, 161.80, 161.29, 157.80, 157.40, 155.10, 149.56, 144.75, 140.58, 134.05, 131.17, 130.24, 123.74, 123.04, 121.81, 120.42, 117.67, 117.34, 114.37, 114.14, 109.76, 87.52; LCMS (+APCI, m/z): 398 (M+H)<sup>+</sup>.

**2-amino-6-(2-fluorophenyl)-4-(3-hydroxy-4-phenoxyphenyl) nicotinonitrile (3l)**

Yield=0.39 g (45%); mp=182–183 °C;  $R_f$  = 0.72 (hexane: ethyl acetate = 8:2); IR (KBr, cm<sup>-1</sup>) = 3491 & 3456 (asym. and sym. stretching of -NH<sub>2</sub>), 3066 (Ar-H), 2218 (C≡N stretching); <sup>1</sup>H NMR (400 MHz, DMSO-*d*<sub>6</sub>) δ 10.00 (s, 1H, OH), 7.96–6.90 (m, 15H, Ar-H+NH<sub>2</sub>); <sup>13</sup>C NMR (101 MHz, DMSO) δ 161.37, 160.72, 157.73, 155.55, 154.49, 149.65, 145.47, 144.84, 134.76, 133.90, 132.31, 132.22, 131.43, 130.24, 123.06, 121.87, 120.19, 119.49, 117.40, 113.14, 110.25, 87.37; LCMS(+APCI, m/z): 398 (M+H)<sup>+</sup>.

**2-amino-6-(4-bromophenyl)-4-(3-hydroxy-4-phenoxyphenyl) nicotinonitrile (3m)**

Yield=0.57 g (65%); mp=146–147 °C;  $R_f$  = 0.82 (hexane: ethyl acetate = 8:2); IR (KBr, cm<sup>-1</sup>) = 3496 and 3392 (asym. and sym. stretching of -NH<sub>2</sub>), 3062 (Ar-H), 2218 (C≡N stretching); <sup>1</sup>H NMR (400 MHz, DMSO-*d*<sub>6</sub>) δ 9.96 (s, 1H, OH), 8.55–6.91 (m,

15H, Ar-H+NH<sub>2</sub>); <sup>13</sup>C NMR (101 MHz, DMSO) δ 161.35, 157.81, 157.73, 155.05, 149.57, 144.73, 137.17, 134.10, 132.10, 130.24, 129.73, 124.30, 123.03, 121.84, 120.38, 117.62, 117.44, 117.33, 109.47, 87.26; LCMS (+APCI, m/z): 459 (M+H)<sup>+</sup>.

**2-amino-6-(3-bromophenyl)-4-(3-hydroxy-4-phenoxyphenyl) nicotinonitrile (3n)** Yield = 0.48 g (55%); mp = 175–176 °C; *R*<sub>f</sub> = 0.80 (hexane: ethyl acetate = 8:2); IR (KBr, cm<sup>-1</sup>) = 3468 and 3361 (asym. and sym. stretching of -NH<sub>2</sub>), 3068 (Ar-H), 2214 (C≡N stretching); <sup>1</sup>H NMR (400 MHz, DMSO-*d*<sub>6</sub>) δ 9.98 (s, 1H, OH), 8.38–6.96 (m, 15H, Ar-H+NH<sub>2</sub>); <sup>13</sup>C NMR (101 MHz, DMSO) δ 161.30, 157.82, 157.14, 155.13, 149.56, 144.76, 140.29, 134.03, 133.18, 131.28, 130.23, 129.14, 126.65, 123.03, 122.71, 121.81, 120.43, 118.19, 117.69, 117.34, 109.74, 87.59; LCMS(+APCI, m/z): 459 (M+H)<sup>+</sup>.

**2-amino-6-(2-bromophenyl)-4-(3-hydroxy-4-phenoxyphenyl) nicotinonitrile (3o)** Yield = 0.39 g (45%); mp = 184–185 °C; *R*<sub>f</sub> = 0.79 (hexane: ethyl acetate = 8:2); IR (KBr, cm<sup>-1</sup>) = 3388 and 3321 (asym. and sym. stretching of -NH<sub>2</sub>), 3230 (Ar-H), 2216 (C≡N stretching); <sup>1</sup>H NMR (400 MHz, DMSO-*d*<sub>6</sub>): 9.98 (s, 1H, OH), 7.75–6.86 (m, 15H, Ar-H+NH<sub>2</sub>); <sup>13</sup>C NMR (100.64 MHz, DMSO-*d*<sub>6</sub>): 161.42, 160.93, 157.70, 153.80, 149.63, 144.93, 140.67, 133.71, 133.51, 131.57, 131.08, 130.23, 128.20, 123.09, 121.77, 121.15, 120.22, 117.47, 117.26, 117.11, 113.50, 87.03; LCMS (+ESI, m/z): 459 (M+H)<sup>+</sup>.

**2-amino-4-(3-hydroxy-4-phenoxyphenyl)-6-(4-hydroxyphenyl) nicotinonitrile (3p)** Yield = 0.57 g (65%); mp = 158–159 °C; *R*<sub>f</sub> = 0.70 (hexane: ethyl acetate = 8:2); IR (KBr, cm<sup>-1</sup>) = 3502 (Ar-OH stretching), 3387 and 3358 (asym. and sym. stretching of -NH<sub>2</sub>), 3076 (Ar-H), 2218 (C≡N stretching); <sup>1</sup>H NMR (400 MHz, DMSO-*d*<sub>6</sub>): 9.95 (s, 2H, 2OH), 8.02–6.83 (m, 15H, Ar-H+NH<sub>2</sub>); <sup>13</sup>C NMR (100.64 MHz, DMSO-*d*<sub>6</sub>): 161.33, 160.04, 159.05, 157.86, 154.44, 149.58, 144.53, 134.50, 130.23, 129.41, 128.80, 122.98, 121.87, 120.25, 117.84, 117.54, 117.28, 115.89, 108.48, 85.53; LCMS (+ESI, m/z): 396 (M+H)<sup>+</sup>.

**2-amino-4-(3-hydroxy-4-phenoxyphenyl)-6-(3-hydroxyphenyl) nicotinonitrile (3q)** Yield = 0.63 g (63%); mp = 178–179 °C; *R*<sub>f</sub> = 0.69 (hexane: ethyl acetate = 8:2); IR (KBr, cm<sup>-1</sup>) = 3464 and 3369 (asym. and sym. stretching of -NH<sub>2</sub>), 3070 (Ar C-H), 2210 (C≡N stretching); <sup>1</sup>H NMR (400 MHz, DMSO-*d*<sub>6</sub>): 9.95 (s, 1H, OH), 9.61 (s, 1H, OH), 7.57–6.84 (m, 15H, Ar-H+NH<sub>2</sub>); <sup>13</sup>C NMR (100.64 MHz, DMSO-*d*<sub>6</sub>): 161.32, 160.24, 159.18, 158.12, 157.81, 154.67, 149.56, 144.72, 139.46, 134.22, 130.23, 130.12, 123.04, 121.81, 120.28, 118.52, 117.63, 117.54, 117.36, 114.44, 109.61, 86.84; LCMS (+ESI, m/z): 396 (M+H)<sup>+</sup>.

## Biological evaluation

### Cell viability assay

MTT assay was executed for the synthesized compounds as per the standardized procedure. HepG2, A-549 and Vero cell lines were used in this study. At first, stock solution of the test compounds and standard compounds (positive control) was prepared in DMSO, and then it was diluted with DMEM (1% antibiotic–antimycotic solution was added) to get the desired concentration before the experiment. The final DMSO concentration was 0.2% in each well which was found to be non-toxic. The cells 5 × 10<sup>3</sup> cells/100 μL were plated in 96-well plates where each cell contained 100 μL DMEM containing 10% FBS and were incubated. The final concentration of the compounds was kept to be (400, 200, 100, 50, 25 μg/ml) starting from the first row. After 24 h, medium was removed and varying concentrations of test compounds were added in 96-well plates. The plates were again incubated for 48 h at 37 °C. After 48 h, sample solution was removed, 10 μl MTT reagent [5 mg/mL in PBS (phosphate-buffered saline)] was added and the cells were incubated for 3 h. After incubation, DMSO was added to solubilize the formed formazan crystals and the sample absorbance was measured at 540 nm using microplate ELISA reader (ELx800, BioTek Instruments Inc., Winooski, VT, USA [30, 31]).

### AO/EB staining method

A-549 cells at the final concentration of 5 × 10<sup>4</sup> cells/well were added to 24-well plates with DMEM containing 10% FBS and were incubated for 24 h. Further, the synthesized compounds were added to the cells at concentration corresponding to their IC<sub>50</sub> and incubated for 48 h. After incubation, about 1–2 mL of PBS was added to wash the cells followed by addition of 1 mL of ice-cold methanol to fix the cells. After 20 min, the methanol was removed and the cells were washed with PBS (2 mL). 300 μL of dual stain AO/EB (20/30 μg/mL dissolved in PBS) was added to every well, and the plates were incubated at 37 °C for 20 min. Finally, PBS was used to wash the plates which was then examined using a fluorescent microscope (Eclipse TS100-F, Nikon Instruments Inc., Melville, NY, USA) to visualize the changes in the morphology of the cell nucleus [32, 33].

### DNA fragmentation assay

DNA fragmentation assay was carried out in vitro as per the standardized protocol [34, 35]. In brief, A549 cell lines were treated with compounds **3b** and **3p**. After incubation for 48 h, the cells were lysed with trypsin and proteinase K and RNase were added to precipitate the DNA. The DNA pellet obtained was dispersed in 100 μL TE buffer (Tris buffer).

The DNA was analyzed on 1.5% agarose gel electrophoresis. The cleaved DNA pattern was visualized at 365 nm UV transilluminator.

### Cell cycle analysis

The mechanism for cytotoxicity by the synthesized compounds on the human lung cancer A549 was determined through flow cytometry. Briefly, the cells were treated with synthesized compounds and incubated for 24 h. Further cells were trypsinized, centrifuged, washed with PBS, ice-cold methanol was added to fix the cell pellets and they were kept at  $-20^{\circ}\text{C}$  for 24 h. Then, PBS was added to wash the cell pellets followed by isotonic PI solution (25  $\mu\text{g}/\text{mL}$  propidium iodide, 0.03% NP-40 and 40  $\mu\text{g}/\text{mL}$  RNase) for cell staining. The cells analysis was done using Accuri C6 flow cytometer (BD Biosciences, San Jose, CA, USA). For every sample, a minimum of 10,000 events was achieved and data analysis was carried out using BD Accuri™ C6 software [33, 36, 37].

### Molecular docking

Schrodinger small-molecule drug discovery suite with Maestro 11.04 interface was used for the molecular docking simulations. Here, X-ray crystal structure of enoyl-acyl carrier protein-reductase domain from human fatty acid synthase (PDB entry: 4W82) of resolution  $1.7 \text{ \AA}$  was taken from PDB ([www.rcsb.org](http://www.rcsb.org)). First, the protein preparation was done using protein preparation wizard (Maestro 11.04, Schrodinger LLC, USA 2017-4). The protein optimization was done by adding hydrogens, deleting water molecules with less than three H-bonds from the protein and assigning the bond order. OPLS 2003 force field is used for the energy minimization to root-mean-square deviation (RMSD) of  $0.30 \text{ \AA}$ . The three-dimensional structures of ligands were drawn by using the 2D sketcher application in maestro. The ligand preparation was carried out by using LigPrep application (version 44011) of Maestro 11.04 with default parameters and ligand energy minimization by using OPLS 2003. The binding site for the ligands on the prepared protein was generated by using site map tool (Schrodinger release 2017-4). Glide module version 77011, schrodinger release 2017-4 was utilized for ligands docking with xtra precision mode (XP) and standard precision mode (SP) at the predicted binding site of the target protein, and final score was obtained through glide multi-ligand scoring function [27, 28, 38].

### Drug likeness (Lipinski's rule of five)

The QikProp application v 5.4, Schrodinger release 2017-4 was used to evaluate the drug-likeness properties of the compounds as per the Lipinski's rule of five. This tool predicts

ADME properties and toxicity of the compounds in silico [38].

### Molecular mechanics: generalized born surface area (MMGBSA)

MMGBSA is a very useful tool for predicting good binding poses and estimation of binding free energies in three-dimensional space. This was done using prime module of the Schrodinger suite—molecular mechanics—generalized born surface area (Prime MM—GBSA v 3.000—Schrodinger 2017-4). The following formula is used for calculating binding free energy [28, 38, 39]:

$$\Delta G_{\text{bin}} = \Delta E_{\text{mm}} + \Delta G_{\text{sol}} + \Delta G_{\text{SA}},$$

where  $\Delta E_{\text{mm}}$  is the difference in the minimized energy between the 4W82 and ligand complex and the total of the energies of the free 4W82 and the free ligands.  $\Delta G_{\text{sol}}$  is the difference in the GBSA solvation energy between the 4W82 and ligand complex and the total of the energies of the free 4W82 and the free ligands.  $\Delta G_{\text{SA}}$  is the difference in the surface energy between the 4w82 and ligand complex and the total of the energies of the free 4W82 and the free ligands.

**Acknowledgements** The authors wish to thank Manipal College of Pharmaceutical Sciences and Manipal Academy of Higher Education for providing the infrastructure facility to carry out this work.

### Compliance with ethical standards

**Conflict of interest** The authors declare that there is no conflict of interest.

### References

1. Biemar F, Foti M (2013) Global progress against cancer—challenges and opportunities. *Cancer Biol Med* 10:183–186. <https://doi.org/10.7497/j.issn.2095-3941.2013.04.001>
2. Kamb A, Wee S, Lengauer C (2007) Why is cancer drug discovery so difficult? *Nat Rev Drug Discov* 6:115–120. <https://doi.org/10.1038/nrd2155>
3. Cancer - fact sheet (2018). World Health Organization. <http://www.who.int/mediacentre/factsheets/fs297/en/>. Accessed 28 Feb 2018
4. Takiar R, Nadial D, Nandakumar A (2010) Projections of Number of Cancer Cases in India (2010–2020) by Cancer Groups. *Asian Pac J Cancer Prev* 11:1045–1049
5. Nawaz K, Webster RM (2016) The non-small-cell lung cancer drug market. *Nat Rev Drug Discov* 15(4):229–230. <https://doi.org/10.1038/nrd.2016.42>
6. Ali R, Mirza Z, Ashraf GMD, Kamal MA, Ansari SA, Damanhour GA, Abuzenadah AM, Chaudhary AG, Sheikh IA (2012) New anti-cancer agents: recent developments in tumor therapy. *Anticancer Res* 32:2999–3005
7. Sadowski MC, Pouwer RH, Gunter JH, Lubik AA, Quinn RJ, Nelson CC (2014) The fatty acid synthase inhibitor triclosan: repurposing an anti-microbial agent for targeting prostate cancer.

- Oncotarget 5:9362–9381. <https://doi.org/10.18632/oncotarget.2433>
8. Sippel KH, Vyas NK, Zhang W, Sankaran B, Quioco FA (2014) Crystal structure of the human fatty acid synthase enoyl-acyl carrier protein-reductase domain complexed with triclosan reveals allosteric protein-protein interface inhibition. *J Biol Chem* 289:33287–33295. <https://doi.org/10.1074/jbc.M114.608547>
  9. Deepa PR, Vandhana S, Muthukumaran S, Umashankar V, Jayanthi U, Krishnakumar S (2010) Chemical inhibition of fatty acid synthase: molecular docking analysis and biochemical validation in ocular cancer cells. *J Ocul Biol Dis Infor* 3:117–128. <https://doi.org/10.1007/s12177-011-9065-7>
  10. Chakravarty B, Gu Z, Chirala SS, Wakil SJ, Quioco FA (2004) Human fatty acid synthase: structure and substrate selectivity of the thioesterase domain. *Proc Natl Acad Sci USA* 101:15567–15572. <https://doi.org/10.1073/pnas.0406901101>
  11. Deepa PR, Vandhana S, Jayanthi U, Krishnakumar S (2012) Therapeutic and toxicologic evaluation of anti-lipogenic agents in cancer cells compared with non-neoplastic cells. *Basic Clin Pharmacol Toxicol* 110:494–503. <https://doi.org/10.1111/j.1742-7843.2011.0844.x>
  12. Honkisz E, Zieba-Przybylska D, Wojtowicz AK (2012) The effect of triclosan on hormone secretion and viability of human chorioncarcinoma JEG-3 cells. *Reprod Toxicol* 34:385–392. <https://doi.org/10.1016/j.reprotox.2012.05.094>
  13. Zhang F, Zhao Y, Sun L, Ding L, Gu Y, Gong P (2011) Synthesis and anti-tumor activity of 2-amino-3-cyano-6-(1H-indol-3-yl)-4-phenylpyridine derivatives in vitro. *Eur J Med Chem* 46:3149–3157. <https://doi.org/10.1016/j.ejmech.2011.03.055>
  14. Mohamed SF, Hosnib HM, Amra AE, Abdalla MM (2016) Synthesis of novel substituted pyridines from 1-(3-aminophenyl)-3-(1H-indol-3-yl)prop-2-en-1-one and their anticancer activity. *Russ J Gen Chem* 86:672–680. <https://doi.org/10.1134/S1070363216030269>
  15. Ghorab MM, Al-Said MS (2012) Anticancer activity of novel indenopyridine derivatives. *Arch Pharm Res* 35:987–994. <https://doi.org/10.1007/s12272-012-0605-x>
  16. Abadi AH, Ibrahim TM, Abouzid KM, Jochen L, Heather NT, Bernard DG, Gary AP (2009) Design, synthesis and biological evaluation of novel pyridine derivatives as anticancer agents and phosphodiesterase 3 inhibitors. *Bioorg Med Chem* 17:5974–5982. <https://doi.org/10.1016/j.bmc.2009.06.03>
  17. Zeng L, Ma H, Pan S, You J, Zhang G, Yu Z, Sheng G, Fu J (2016) LINE-1 gene hypomethylation and p16 gene hypermethylation in HepG2 cells induced by low-dose and long-term triclosan exposure: the role of hydroxyl group. *Toxicol Vitro* 34:35–44. <https://doi.org/10.1016/j.tiv.2016.03.002>
  18. Sippel KH, Vyas NK, Zhang W, Sankaran B, Quioco FA (2014) Crystal structure of the human Fatty Acid synthase enoyl-acyl carrier protein-reductase domain complexed with triclosan reveals allosteric protein-protein interface inhibition. *J Biol Chem* 289:33287–33295. <https://doi.org/10.1074/jbc.M114.608547>
  19. Sankar KS, Bhat V, Rao PNP, Shenoy VP, Bairy I, Shenoy G (2016) Rational design and synthesis of novel diphenyl ether derivatives as antitubercular agents. *Drug Des Devel Ther* 10:2299–2310. <https://doi.org/10.2147/DDDT.S104037>
  20. Gouda MA, Berghot MA, Abd El Ghani GE, Khalil AEGM (2014) Chemistry of 2-Amino-3-cyanopyridines. *Synth Commun* 44:297–330. <https://doi.org/10.1080/00397911.2013.823549>
  21. Kalaria PN, Satasia SP, Avalani JR, Raval DK (2014) Ultrasound-assisted one-pot four-component synthesis of novel 2-amino-3-cyanopyridine derivatives bearing 5-imidazopyrazole scaffold and their biological broadcast. *Eur J Med Chem* 83:655–664. <https://doi.org/10.1016/j.ejmech.2014.06.071>
  22. Samarhandian S, Shabestari MM (2013) DNA fragmentation and apoptosis induced by safranal in human prostate cancer cell line. *Indian J Urol* 29:177–183. <https://doi.org/10.4103/0970-1591.117278>
  23. Kihlmark M, Imreh G, Hallberg E (2001) Sequential degradation of proteins from the nuclear envelope during apoptosis. *J Cell Sci* 114:3643–3653
  24. Zhang JH, Xu M (2000) DNA fragmentation in apoptosis. *Cell Res* 10:205–211. <https://doi.org/10.1038/sj.cr.7290049>
  25. Nagata S, Nagase H, Kawane K, Mukae N, Fukuyama H (2003) Degradation of chromosomal DNA during apoptosis. *Cell Death Differ* 10:108–116. <https://doi.org/10.1038/sj.cdd.4401161>
  26. Cecchini MJ, Amiri M, Dick FA (2012) Analysis of cell cycle position in mammalian cells. *J Vis Exp* 59:1–7. <https://doi.org/10.3791/3491>
  27. Sanjay BB, Nitin GH (2017) Design, synthesis and molecular docking study of thienopyrimidin-4(3H)-thiones as antifungal agents. *J Saudi Chem Soc* 21:S264–S274. <https://doi.org/10.1016/j.jscs.2014.02.011>
  28. Malikanti R, Vadija R, Veeravaran H, Mustyala KK, Malkhed V, Vuruputuri U (2017) Identification of small molecular ligands as potent inhibitors of fatty acid metabolism in *Mycobacterium tuberculosis*. *J Mol Struct* 1150:227–241. <https://doi.org/10.1016/j.molstruc.2017.08.090>
  29. Gillmore A, Lauret C, Roberts SM (2003) A route to the structure proposed for puetuberosanol and approaches to the natural products marshrin and phebalsin. *Tetrahedron* 59:4363–4375. [https://doi.org/10.1016/S0040-4020\(03\)00624-0](https://doi.org/10.1016/S0040-4020(03)00624-0)
  30. Florento L, Matias R, Tũaño E, Santiago K, Dela Cruz F, Tuazon A (2012) Comparison of cytotoxic activity of anticancer drugs against various human tumor cell lines using in vitro cell-based approach. *Int J Biomed Sci* 8:76–80
  31. Aliabadi A, Eghbalian E, Kiani A (2013) Synthesis and evaluation of the cytotoxicity of a series of 1,3,4-thiadiazole based compounds as anticancer agents. *Iran J Basic Med Sci* 16:1133–1138
  32. Bomfim DS, Ferraz RPC, Carvalho NC, Soares MBP, Pinheiro MLB, Costa EV, Bezerra DP (2013) Eudesmol isomers induce caspase-mediated apoptosis in human hepatocellular carcinoma HepG2 cells. *Basic Clin Pharmacol Toxicol* 113:300–306. <https://doi.org/10.1111/bcpt.12097>
  33. Aryapour H, Riaz GH, Ahmadian S, Foroumadi A, Mahdavi M, Emami S (2012) Induction of apoptosis through tubulin inhibition in human cancer cells by new chromene-based chalcones. *Pharm Biol* 50:1551–1560. <https://doi.org/10.3109/13880209.2012.695799>
  34. Gouthamchandra K, Sudeep HV, Venkatesh BJ, Prasad KS (2017) Chlorogenic acid complex (CGA7), standardized extract from green coffee beans exerts anticancer effects against cultured human colon cancer HCT-116 cells. *Food Sci Hum Wellness* 6:147–153. <https://doi.org/10.1016/j.fshw.2017.06.01>
  35. Mukherjee S, Mitra I, Reddy BVP, Fouzder C, Mukherjee S, Ghosh S, Chatterji U, Moi SC (2017) Effect of Pt(II) complexes on cancer and normal cells compared to clinically used anticancer drugs: cell cycle analysis, apoptosis and DNA/BSA binding study. *J Mol Liq* 247:126–140. <https://doi.org/10.1016/j.molliq.2017.09.014>
  36. Gooch JL, Yee D (1999) Strain-specific differences in formation of apoptotic DNA ladders in MCF-7 breast cancer cells. *Cancer Lett* 144:31–37. [https://doi.org/10.1016/S0304-3835\(99\)00208-6](https://doi.org/10.1016/S0304-3835(99)00208-6)
  37. Prabhu S, Vijayakumar S, Swaminathan K, Manogar P (2018) Antidiabetic activity of quercetin extracted from *Phyllanthus emblica* L. fruit: in silico and in vivo approaches. *J Pharm Anal* 8:109–118. <https://doi.org/10.1016/j.jpha.2017.10.005>
  38. Sharma A, Gudala S, Ambati SR, Penta S, Bomma Y, Janapala VR, Jha A, Kumar A (2018) Synthesis, Anticancer Evaluation, and Molecular Docking Studies of Novel (4-Hydroxy-2-Thioxo-3,4-Dihydro-2H-[1, 3]Thiazin-6-Yl)-Chromen-2-Ones via a Multicomponent Approach. *J Chin Chem Soc* 65:810–821. <https://doi.org/10.1002/jccs.201700340>